

Article

Grating Coupler Design for Vertical Light Coupling in Silicon Thin Films on Lithium Niobate

Huangpu Han ^{1,2} and Bingxi Xiang ^{3,*} 

¹ College of Electric and Electronic Engineering, Zibo Vocational Institute, Zibo 255314, China; 12077@zbcvc.edu.cn

² School of Physics, Shandong University, Jinan 250100, China

³ College of New Materials and New Energies, Shenzhen Technology University, Shenzhen 518118, China

* Correspondence: xiangbingxi@sztu.edu.cn; Tel.: +86-135-3085-0236

Received: 10 August 2020; Accepted: 21 September 2020; Published: 22 September 2020



Abstract: In this paper we provide a design for a vertical grating coupler for a silicon thin film on lithium niobate. The parameters—such as the cladding layer thickness of lithium niobate, fiber position, fiber angle, grating period, and duty cycle—are analyzed and optimized to reduce the mode mismatch loss and the internal reflections. The alignment tolerances, for the grating coupler parameters, are also simulated and evaluated. We determine that our simulated grating coupler exhibits high efficiency, enhanced light coupling, and high alignment tolerance.

Keywords: grating coupler; thin film; integrated optics; 3D-FDTD

1. Introduction

In dense photonic integration, highly developed silicon (Si) platforms have attained numerous substantial successes. The advantages of this mature technology are their low optical absorption, large refractive index contrast, and high compatibility with semiconductor technology [1]. However, single-crystal Si is a centrally symmetric crystal that has no linear electro-optic effect, piezo-electric or other similar properties. As a result, the Si material has limitations in its application to integrated optics. An alternative is lithium niobate (LiNbO₃, LN) crystal, which is more promising in this role [2–4] because of its wide transparency range and excellent electro-optic, nonlinear, acousto-optic, piezoelectric, photorefractive, and elasto-optic properties. However, contrary to photonics based on Si, the manufacturing of LN photonic devices is still in its infancy. The integration of a Si thin film on a thin LN cladding layer, combines the mature micro- and nano- technology properties of Si and the optical properties of LN. This produces an enhanced optical material that has a good confinement, and strong guidance, of light due to the high-refractive-index contrast between Si and LN [5,6]. When the light propagates in the Si waveguide, the energy of the light is distributed within both the Si thin film and the LN layer. Electro-optic modulators in Si on LN can be prepared by applying voltage to the LN layer [7–11]. Previously, based on a hybrid Si/LN material, many photonic devices have been developed such as Mach-Zehnder interferometer [7,8], photonic crystals [9] and micro-ring resonator [10,11].

Due to the substantial light mode mismatch between the sub-micron-sized optical material devices and single-mode fibers, the coupling efficiency between them is very low; this will impede improvement in performance of the optical device. An effective method, which requires no end-face polishing, for the coupling of fibers and optical devices is known as grating coupling [12–17]. Many previous articles report on the grating coupler in silicon on insulator (SOI) [12–14] and lithium niobate on insulator (LNOI) [15–17], but few reports investigate a grating coupler for a Si thin film on LN.

In this study, a grating coupler for a Si thin film on LN was simulated and analyzed. This scheme, based on the three-dimension finite-difference time-domain method (3D-FDTD) [18], involved the

cladding layer thickness of LN thin film (T), fiber position x (separation of the x -axis between grating edge and the fiber core, Lx), fiber position y (separation of the y -axis between grating upper surface and the fiber core, Ly), fiber position z (separation of the z -axis between grating centerline and the fiber core, Lz), fiber angle (θ), grating period (Λ), and duty cycle (DC , defined as the fraction of the ridge width within the period). All these parameters were investigated so that guidance on the improvement of the coupling efficiency of the grating coupler could be provided. The tolerances of the grating coupler, which was significantly important for any practical implementation of such a device, were also carefully studied.

2. Device Design and Methods

The Si thin film on LN that was studied moving from the highest to the lowest layer involved a $0.22\ \mu\text{m}$ -thick Si thin film [19,20], a z-cut LN film, and a Si substrate. The schematic cross-section of which, including the grating coupler is shown in Figure 1. We simulated coupling process between the optical fiber and the grating coupler for the fiber fundamental transverse electric mode (TE_0) as a source. In this simulation, the thickness of the Si thin film and the etch depth were all chosen to be $0.22\ \mu\text{m}$; the parameters T , Lx , Ly , Lz , θ , Λ , and DC were varied to maximize the light from the single-mode fiber coupling into the waveguide.

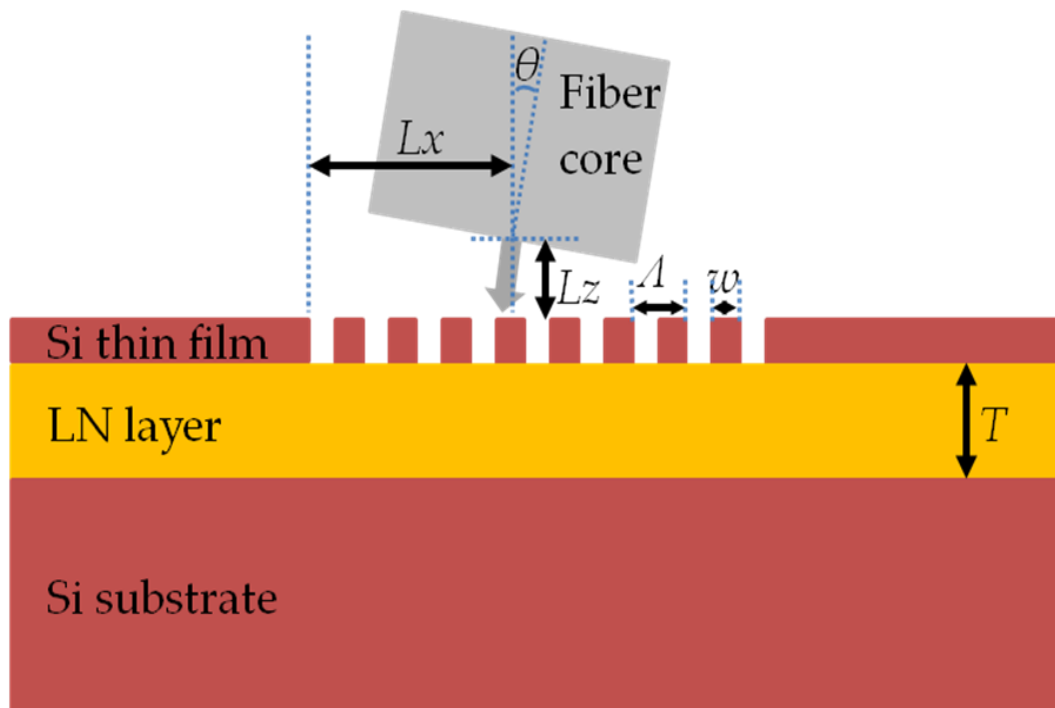


Figure 1. Schematic cross-section of a grating coupler in Si thin film on LN.

The Bragg phase matching condition was the basic equation of grating couplers. The coupling modes were resonantly excited when the conditions were met. For an infinitely long grating, the equation was given by [21]:

$$k \sin\theta = \beta + q2\pi/\Lambda, \quad (1)$$

where $k = 2\pi/\lambda$ is the wavenumber, θ is the incident angle, q is the diffraction order (here $q = -1$), Λ is the grating period, $\beta = 2\pi n_{\text{eff}}/\lambda$ is the real part of the propagation constant and n_{eff} is the effective index of the guided mode in the grating coupler. The above equation was used to obtain the range of grating periods (Λ).

In order to avoid a high second order reflection at the grating-waveguide interface, θ was chosen to be 8° [21]. The effective refractive index should fulfill the inequality $n_{\text{LN}} \leq n_{\text{eff}} \leq n_{\text{Si}}$, where $n_{\text{LN}}/n_{\text{Si}}$

was the refractive index of LN (2.138)/Si (3.478). By substituting the inequality into Equation (1), an estimated range of Λ with respect to the fiber angle would be obtained: $\lambda/(3.478 - \sin\theta) \leq \Lambda \leq \lambda/(2.138 - \sin\theta)$. The Λ could be in the estimated range of $0.465 \mu\text{m} \leq \Lambda \leq 0.775 \mu\text{m}$.

The grating coupling mechanism was shown as follows: light was coupled in the waveguide plane, from the single-mode fiber, due to the diffraction effect of the grating coupled to the periodic grating structure; when the input field mode was adjusted to match the fiber mode, light coupled effectively into the waveguide plane from the single-mode fiber. Coupling efficiency was defined as the ratio of the power converted to the waveguide plane to the source power. The parameters for the grating coupler were optimized to reduce the mode mismatch between the waveguide optical devices and the single-mode fibers. We performed simulations and optimizations using a 3D-FDTD method and a perfectly matched layer (PML) boundary conditions [22].

3. Results and Discussion

To determine an enhanced coupling efficiency, the parameters for the design of the grating coupler need to be carefully analyzed. At a wavelength of light of $1.55 \mu\text{m}$, a Si thin film thickness of $0.22 \mu\text{m}$, and an etch depth of $0.22 \mu\text{m}$, the parameters of the grating coupler for TE polarization were simulated and optimized. The results of which are shown in Table 1. In this work, the control variable method was used to study the influence of each parameter on the performance of the grating coupler. During the simulation, other parameters were fixed to their optimized value and only the studied parameters were modified.

Table 1. Optimized parameters for the grating coupler for TE polarization ($\lambda = 1.55 \mu\text{m}$).

| T (μm) | L_x (μm) | L_y (μm) | θ ($^\circ$) | Λ (μm) | DC |
|-----------------------|-------------------------|-------------------------|-----------------------|-----------------------------|-------|
| 2.1 | 3.5 | 0 | 8 | 0.64 | 0.829 |

Figure 2 shows the relationship between the coupling efficiency and thickness of the LN cladding layer for a TE polarization. With varying cladding layer thickness of the LN, the curve of coupling efficiency oscillated between the minimum and the maximum, as described in [23] and [24]. A possible reason for this was explained as follows. As a beam of light from the fiber was diffracted by the grating coupler, part of the light beam was scattered towards the LN cladding layer. At the LN/Si substrate interface, a part of the power was transmitted into the Si substrate and a part of it was reflected. The reflected part propagated upward again through the LN cladding layer toward grating. The LN cladding layer thickness should be chosen such that the reflected light and the incident light met the phase matching condition. The T at high coupling efficiency was determined via the parameters of L_x , L_y , L_z , θ , Λ , DC , λ , etc. In the following simulation, the T was selected to be $2.1 \mu\text{m}$.

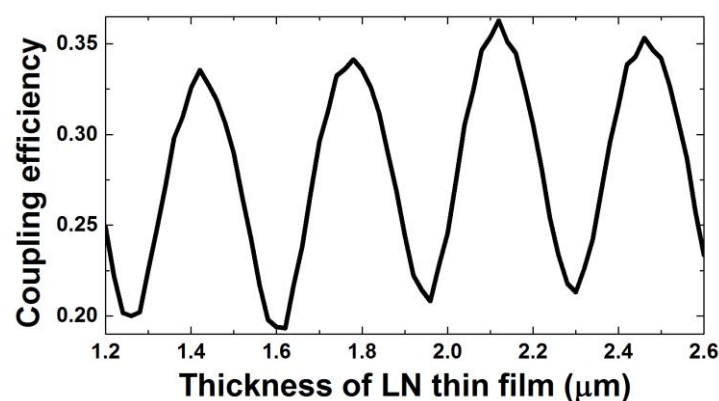


Figure 2. Coupling efficiency at different thicknesses of the LN cladding layer for TE polarization.

To study the tolerance of L_x and L_y , the simulations for the coupling efficiency as a function of wavelength for varying L_x and L_y were performed. Figure 3a,b show this coupling efficiency as a function of L_x and L_y , respectively. When the L_x was set at $3.5 \mu\text{m}$ and L_y was at $0 \mu\text{m}$, the coupling efficiency was at a maximum. With a $2 \mu\text{m}$ deviation in L_x , the coupling efficiency descended a little. When the deviation of L_y was smaller than $4 \mu\text{m}$, the coupling efficiency was almost unchanged; when larger than $4 \mu\text{m}$, the coupling efficiency sharply descended, at an increased rate as the L_y deviation increased. Figure 3c,d corresponding to the red circles in Figure 3a,b show the coupling efficiency as a function of wavelength for different L_x and L_y , respectively. For an increasing wavelength, the coupling efficiency increased at first and but then decreased after reaching the peak at a wavelength of $1.55 \mu\text{m}$.

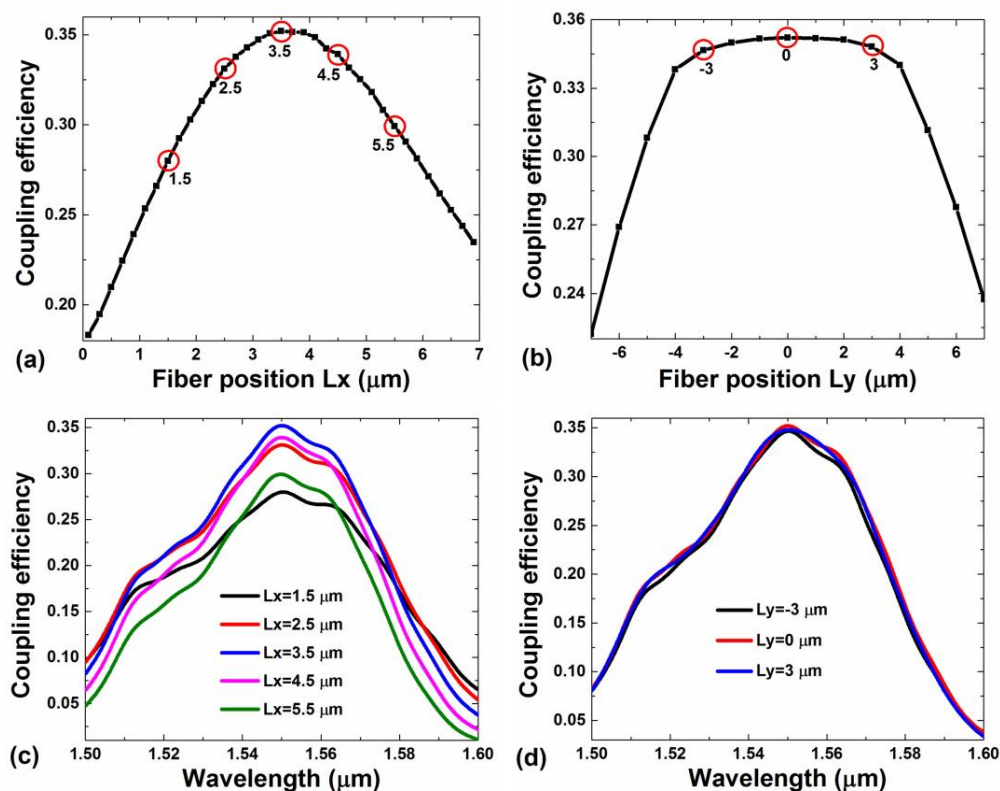


Figure 3. Coupling efficiency as a function of L_x (a) and L_y (b) and: coupling efficiency as a function of wavelength for different L_x (c) and L_y (d).

Figure 4 shows this coupling efficiency as a function of L_z . When L_z was smaller than $8 \mu\text{m}$, the curve of coupling efficiency had little fluctuation. When L_z was larger than $8 \mu\text{m}$, the coupling efficiency descended because light from fiber to grating scattered.

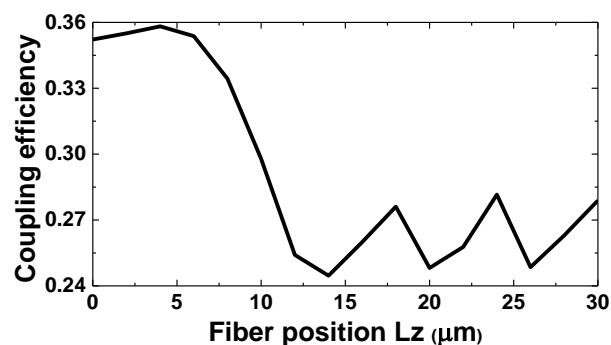


Figure 4. Coupling efficiency as a function of L_z .

Figure 5a illustrates the coupling efficiency as a function of fiber angle. To reduce back reflections, the incident angle was optimized at 8° in Figure 5a. With an increasing deviation from this fiber angle, the coupling efficiency descended slowly. Figure 5b shows coupling efficiency as a function of wavelength for different fiber angles, corresponds to the red circles in Figure 5a. At $\lambda = 1.55 \mu\text{m}$, for incident angle $\theta = 3^\circ, 8^\circ$, and 13° , the coupling efficiencies were 34.17%, 35.21%, and 34.71%, respectively.

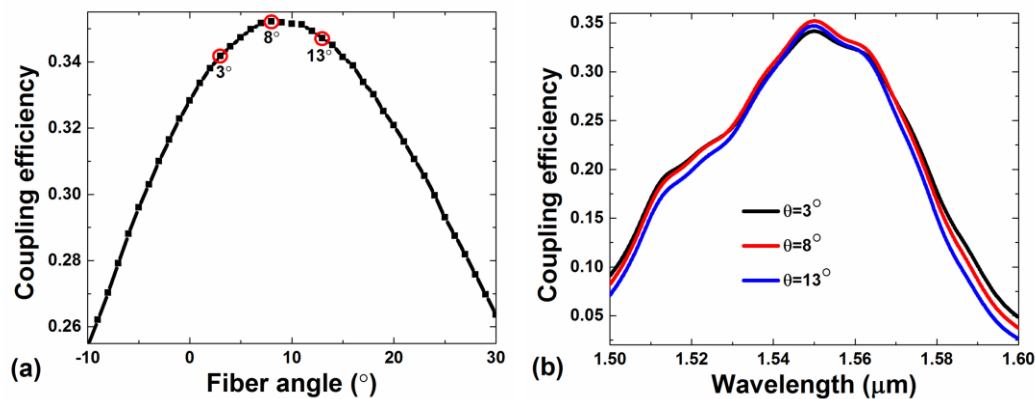


Figure 5. (a) Coupling efficiency as a function of fiber angle, which is relative to the surface that is perpendicular to the Si substrate. (b) Coupling efficiency as a function of wavelength for different fiber angles. ($T = 2.1 \mu\text{m}$, $Lx = 3.5 \mu\text{m}$, $Ly = 0 \mu\text{m}$, $\Lambda = 0.64 \mu\text{m}$, and $DC = 0.829$).

Coupling efficiency as a function of period is shown in Figure 6a. A grating period of $0.64 \mu\text{m}$ provided the peak coupling efficiency; the coupling efficiency decreased whenever the grating period increased or decreased from this position. When the grating period deviated by 0.004 and $0.008 \mu\text{m}$, the coupling efficiency decreased a minuscule amount at a wavelength of $1.55 \mu\text{m}$. Figure 6b shows coupling efficiency as a function of wavelength for different periods, which corresponds to the red circles in Figure 6a. The peak coupling efficiency was red shifted with an increasing period.

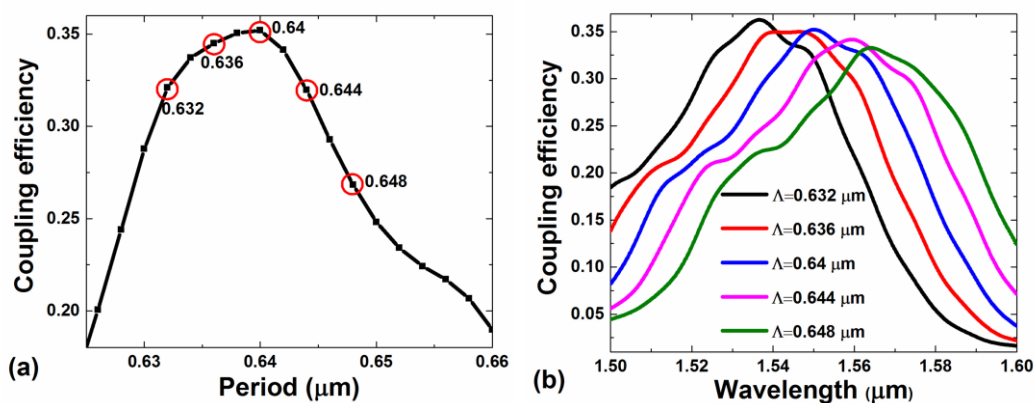


Figure 6. (a) Coupling efficiency as a function of period. (b) Coupling efficiency as a function of wavelength for different period.

Coupling efficiency as a function of duty cycle is illustrated in Figure 7a. A grating duty cycle of 0.829 provided a peak coupling efficiency. For 0.019 and 0.021 deviation of the duty cycle at a wavelength of $1.55 \mu\text{m}$, the change in coupling efficiency was tiny. Figure 7b shows the coupling efficiency as a function of wavelength for different duty cycle, corresponds to the red circles in Figure 7a. The peak coupling efficiency was red shifted with an increasing duty cycle.

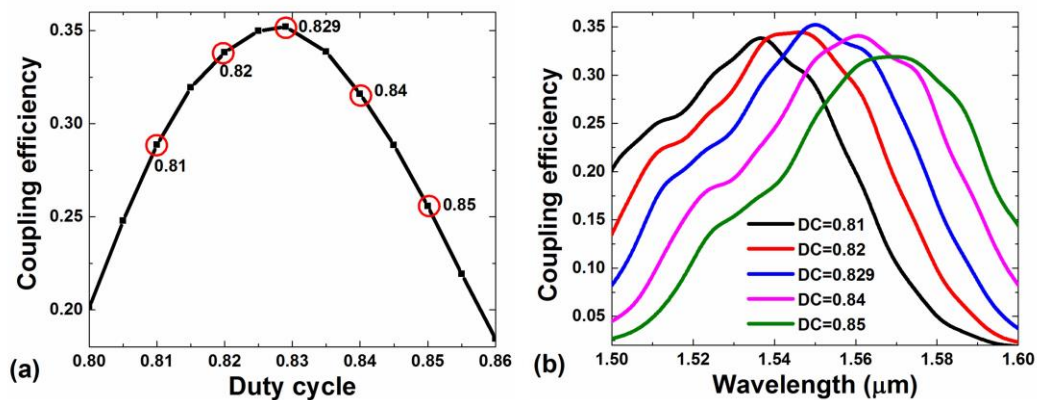


Figure 7. (a) Coupling efficiency as a function of duty cycle. (b) Coupling efficiency as a function of wavelength for different duty cycle.

The electric field distribution is shown in Figure 8. The in-coupled light formed an angle (8°) relative to the surface that was perpendicular to the Si substrate. Grating couplers that operated at around $1.55 \mu\text{m}$ could achieve near-vertical coupling with the waveguide plane also and avoid a high amount of reflection. The light was mainly divided into three parts: one scattered upwards, one coupled into the waveguide, and the other lost into the substrate.

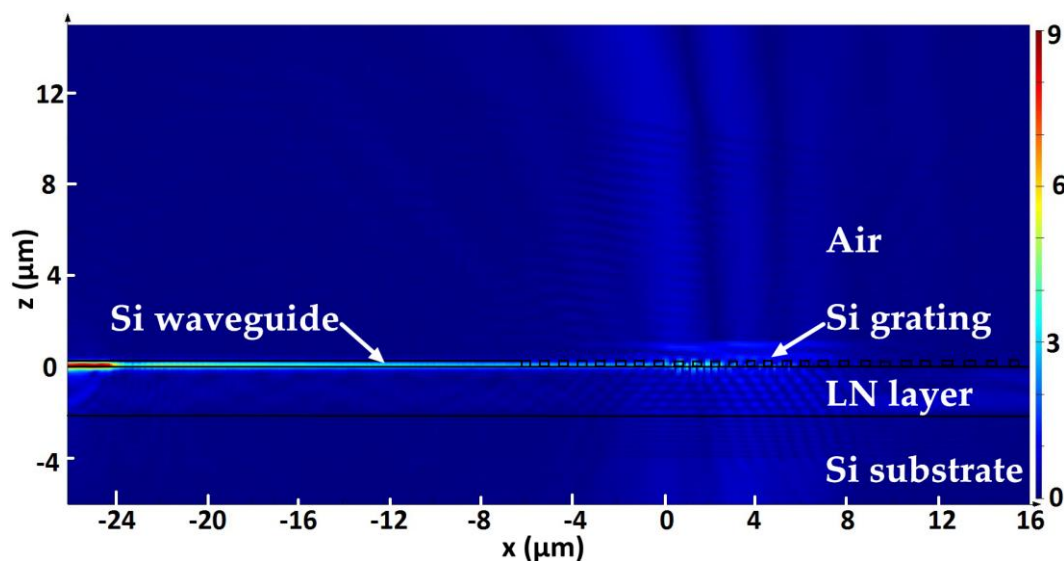


Figure 8. Electric field distribution of the optical wave in the simulation region, in which the optimal values of $T = 2.1 \mu\text{m}$, $L_x = 3.5 \mu\text{m}$, $L_y = 0 \mu\text{m}$, $\theta = 8^\circ$, $\Lambda = 0.64 \mu\text{m}$, $DC = 0.829$, and $\lambda = 1.55 \mu\text{m}$ were employed.

4. Conclusions

In conclusion, the performance of a grating coupler, with vertical light coupling, from a single-mode fiber to a waveguide in a $0.22 \mu\text{m}$ -thick Si thin film on LN was systematically studied by using a 3D-FDTD simulation technique. The parameters T , L_x , L_y , θ , Λ , and DC were analyzed and found to be optimized at $2.1 \mu\text{m}$, $3.5 \mu\text{m}$, $0 \mu\text{m}$, 8° , $0.64 \mu\text{m}$, and 0.829 , respectively. A maximum of 35.2% was found for the coupling efficiency. The tolerances of the grating coupler parameters were discussed with respect to the coupling efficiency. A Si thin film on LN is being researched and fabricated at the research centre of Nanoln. Our simulation results on the grating couplers for such an optical device will provide useful guidance to laboratory work such as this.

Author Contributions: B.X. conceived the original idea; H.H. carried out the simulations, analyzed the data, and wrote the paper; B.X. and H.H. contributed the useful and deep discussions and modified the manuscript. All authors have read and agreed to the published version of the manuscript.

Funding: This research was funded by the Shenzhen Science and Technology Planning (NO. JCYJ20190813103207106), the Project of Youth Innovative Talents in Higher Education Institutions of Guangdong (NO. 2018KQNCX399), the Foundation of Zibo Vocational Institute (NO. 2018zzzr03), and the School City Integration Development Plan of Zibo (NO. 2019ZBXC127).

Conflicts of Interest: The authors declare no conflict of interest.

References

1. Witzens, J.; Baehr-Jones, T.; Hochberg, M. Silicon photonics: On-chip OPOs. *Nat. Photonics* **2010**, *4*, 10–12. [[CrossRef](#)]
2. Weis, R.S.; Gaylord, T.K. Lithium niobate: Summary of physical properties and crystal structure. *Appl. Phys. A* **1985**, *37*, 191–203. [[CrossRef](#)]
3. Lawrence, M. Lithium niobate integrated optics. *Rep. Prog. Phys.* **1993**, *56*, 363–429. [[CrossRef](#)]
4. Syms, R.R.A. Advances in channel waveguide lithium niobate integrated optics. *Opt. Quant. Electron.* **1988**, *20*, 189–213. [[CrossRef](#)]
5. Rao, A.; Fathpour, S. Compact lithium niobate electrooptic modulators. *IEEE J. Sel. Top. Quantum Electron.* **2018**, *24*, 340014. [[CrossRef](#)]
6. Rao, A.; Fathpour, S. Heterogeneous thin-film lithium niobate integrated photonics for electrooptics and nonlinear optics. *IEEE J. Sel. Top. Quantum Electron.* **2018**, *24*, 8200912. [[CrossRef](#)]
7. Chiles, J.; Fathpour, S. Mid-infrared integrated waveguide modulators based on silicon-on-lithium-niobate photonics. *Optica* **2014**, *1*, 350–355. [[CrossRef](#)]
8. Cao, L.; Aboketaf, A.; Wang, Z.; Preble, S. Hybrid amorphous silicon (a-Si:H)–LiNbO₃ electro-optic modulator. *Opt. Commun.* **2014**, *330*, 40–44. [[CrossRef](#)]
9. Witmer, J.D.; Hill, J.T.; Safavi-Naeini, A.H. Design of nanobeam photonic crystal resonators for a silicon-on-lithium-niobate platform. *Opt. Express* **2016**, *24*, 5876. [[CrossRef](#)]
10. Witmer, J.D.; Valery, J.A.; Arrangoiz-Arriola, P.; Sarabalis, C.J.; Hill, J.T.; Safavi-Naeini, A.H. High-Q photonic resonators and electro-optic coupling using silicon-on-lithium-niobate. *Sci. Rep.* **2016**, *7*, 46313. [[CrossRef](#)]
11. Han, H.; Xiang, B. Simulation and analysis of electro-optic tunable microring resonators in silicon thin film on lithium niobate. *Sci. Rep.* **2019**, *9*, 6302. [[CrossRef](#)] [[PubMed](#)]
12. Schmid, B.; Petrov, A.; Eich, M. Optimized grating coupler with fully etched slots. *Opt. Express* **2009**, *17*, 11066–11076. [[PubMed](#)]
13. Laere, F.V.; Roelkens, G.; Ayre, M.; Schrauwen, J.; Taillaert, D.; Thourhout, D.V.; Krauss, T.F.; Baets, R. Compact and highly efficient grating couplers between optical fiber and nanophotonic waveguides. *J. Lightw. Technol.* **2007**, *25*, 151–156. [[CrossRef](#)]
14. Roelkens, G.; Vermeulen, D.; Thourhout, D.V.; Baets, R.; Brision, S.; Lyan, P.; Gautier, P.; Fédéli, J.M. High efficiency diffractive grating couplers for interfacing a single mode optical fiber with a nanophotonic silicon-on-insulator waveguide circuit. *Appl. Phys. Lett.* **2008**, *92*, 131101. [[CrossRef](#)]
15. Chen, Z.; Wang, Y.; Jiang, Y.; Kong, R.; Hu, H. Grating coupler on single-crystal lithium niobate thin film. *Opt. Mater.* **2017**, *72*, 136–139. [[CrossRef](#)]
16. Cai, L.; Piazza, G. Low-loss chirped grating for vertical light coupling in lithium niobate on insulator. *J. Opt.* **2019**, *21*, 065801. [[CrossRef](#)]
17. Nisar, M.S.; Zhao, X.; Pan, A.; Yuan, S.; Xia, J. Grating coupler for an on-chip lithium niobate ridge waveguide. *IEEE Photonics J.* **2017**, *9*, 1–8. [[CrossRef](#)]
18. Tavlove, A.; Hagness, S.C. *Computational Electrodynamics: The Finite-Difference Time-Domain Method*, 3rd ed.; Artech House: Norwood, MA, USA, 2005.
19. Matthew, S.; Shi, R.; Novack, A.; Cher, R.T.P.; Lim, A.E.-J.; Lo, P.G.-Q.; Baehr-Jones, T.; Hochberg, M. A compact bi-wavelength polarization splitting grating coupler fabricated in a 220 nm SOI platform. *Opt. Express* **2013**, *21*, 31019–31028.
20. Wang, Y.; Gao, S.; Wang, K.; Li, H.; Skafidas, E. Ultra-broadband, compact, and high-reflectivity circular Bragg grating mirror based on 220 nm silicon-on-insulator platform. *Opt. Express* **2017**, *25*, 6653–6663. [[CrossRef](#)]

21. Vivien, L.; Pascal, D.; Lardenois, S.; Marris-Morini, D.; Cassan, E.; Grillot, F.; Laval, S.; Fédéli, J.-M.; Melhaoui, L.M. Light injection in SOI microwaveguides using high-efficiency grating couplers. *J. Lightw. Technol.* **2006**, *24*, 3810–3814. [[CrossRef](#)]
22. Berenger, J.P. A perfectly matched layer for absorption of electromagnetic wave. *J. Comput. Phys.* **1994**, *114*, 185–200. [[CrossRef](#)]
23. Suhara, T.; Nishihara, H. Integrated optics components and devices using periodic structures. *IEEE J. Quantum Electron.* **1986**, *22*, 845–867. [[CrossRef](#)]
24. Emmons, R.M.; Hall, D.G. Buried-oxide silicon-on-insulator structures. II. Waveguide grating couplers. *IEEE J. Quantum Electron.* **1992**, *28*, 164–175. [[CrossRef](#)]



© 2020 by the authors. Licensee MDPI, Basel, Switzerland. This article is an open access article distributed under the terms and conditions of the Creative Commons Attribution (CC BY) license (<http://creativecommons.org/licenses/by/4.0/>).